Haptic Interface Control – Design Issues and Experiments with a Planar Device

Mohammad R. Sirouspour, S. P. DiMaio, S. E. Salcudean, P. Abolmaesumi and C. Jones
Department of Electrical and Computer Engineering, University of British Columbia
Vancouver, BC, V6T 1Z4, Canada
{*tims@ece.ubc.ca*}

Abstract

This paper describes the haptic rendering of a virtual environment by drawing upon concepts developed in the area of teleoperation. A four-channel teleoperation architecure is shown to be an effective means of coordinating the control of a new 3-DOF haptic interface with the simulation of a virtual dynamic environment.

1 Introduction

The issue of haptically rendering interactive virtual environments is essentially a teleoperation problem in which the haptic interface and the virtual slave are almost always both kinematically and dynamically dissimilar, resulting in some difficulty in realizing transparent interaction between the user and the synthetic environment [11]. For haptic displays, *impedance* and *admittance* simulations have been proposed [1, 2, 13, 8]. Impedance display, the more widespread of the two, passes sensed hand positions to the dynamic simulator, while forces are returned from the environment. This is essentially a two-channel approach. The transmission of positions and forces in both directions between master and slave has been found to be important for achieving high performance in teleoperation systems [6, 11]. In this paper we describe a novel multi-channel architecture for haptic simulation, as well as the use of an explicitly modelled *virtual slave*. A four-channel coupling between the haptic interface and dynamic simulation allows the interface to behave as a force sensor or as a position sensor depending upon the impedance of the virtual environment, and is therefore a hybrid of the two traditionally adopted approaches [11]. This strategy has been evaluated experimentally by means of a haptic simulation in which the user manipulates a virtual slave within a contact environment via a new parallel, redundant device. The haptic interface maintains a large, isotropic workspace while sensing both position and applied hand forces, in accordance with the four-channel control framework. A force/velocity observer is employed for force sensing without additional hardware [4] and is shown to be effective despite using only joint angle measurements and a detailed model of the mechanism dynamics.

The paper begins with a description of the haptic simulation system and is followed by an outline of the haptic device design, its dynamics, actuation and sensing. The interface control and its implementation within the teleoperation framework are detailed and evaluated experimentally. Finally, concluding remarks and scope for future work are presented.

2 Haptic Simulation Architecture

A virtual environment system serves as a test bed for the concepts presented in subsequent sections. It comprises a new planar 3-DOF haptic interface; virtual slave and environment models; a controller that coordinates both force and position information between the haptic interface and the virtual environment; and a graphical display, as depicted in Figure 1. The user manipulates a virtual rectangular block that is contained within an enclosure of virtual rigid walls, rendered by a physically-based contact model [3]. The block has

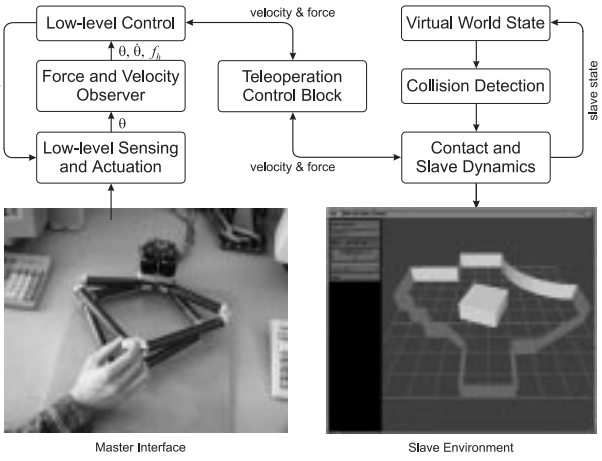

Figure 1: The virtual environment system architecture.

a mass of 2kg and a moment-of-inertia of 0.005kgm^2, which are to be perceived by the human hand as it manipulates the haptic interface.

The real-time control architecture maintains a control loop sampling rate of 1000Hz and is supported by a 400MHz PC running the QNX operating system. The input of joint angles and the output of motor current values is performed by a Quanser Multi-Q-3^{TM} I/O adapter.

3 The Planar Pantograph Haptic Interface

The haptic interface has three degrees of freedom allowing for planar translation and unlimited rotation about a single axis, as shown in Figure 2. The endpoints of two pantographs move in different parallel planes and are coupled by means a linkage connected to the interface handle. The linkage bar forms a crank that allows the handle to rotate unhindered. Each pantograph is driven by two DC motors located at the base joints.

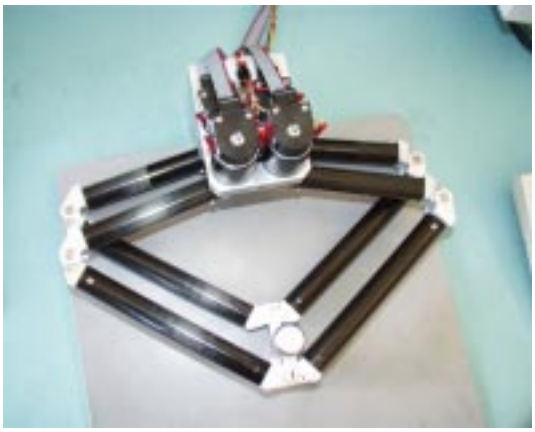

Figure 2: The three-degree-of-freedom planar pantograph interface.

3.1 Mechanism Dynamics

An accurate model of haptic interface dynamics is desirable for control purposes and begins with the derivation of the equations of motion using the Euler-Lagrange approach [12]. Because of the complex parallel structure of the interface and its inherent actuation redundancy, the dynamics of each pantograph mechanism is first described separately and then combined to form a single model. The equations of motion in actuated joint variables, $\theta = [\theta_1 \ \theta_2]^T$, are expressed in terms of the parameters shown in Figure 3:

$$D_p(\theta)\ddot{\theta} + C_p(\theta,\dot{\theta})\dot{\theta} = \tau_p - J_e^T F_e \ , \qquad (1)$$

where τ_p is a vector of the applied actuator torques, J_e is the manipulator Jacobian, and F_e is the hand force applied to the end-effector. Mass and Christoffel matrices D_p and C_p are also present.

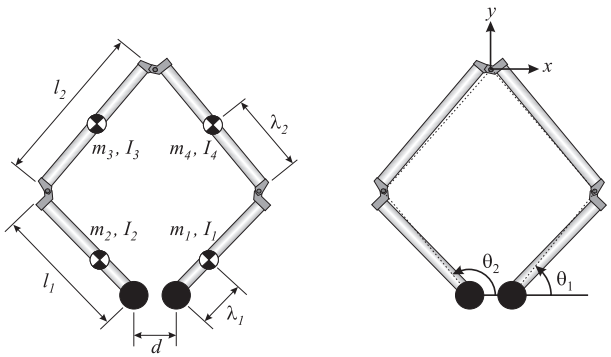

Figure 3: Pantograph configuration and parameters.

The equations of motion describing the workspace dynamics of two coupled pantographs become:

$$M_c\ddot{X}_c + C_c\dot{X}_c = F_h + J_c^T\tau = F_h + u \ , \qquad (2)$$

with $M_c = J_c^T D J_c + M$ and $C_c = J_c^T D\dot{J}_c + J_c^T C J_c$, where X_c is a vector of interface handle coordinates $[x_c \ y_c \ \alpha]$ and D and C are block diagonal matrices that include the mass and Christoffel matrices of each of the two pantographs, respectively. The Jacobian matrix $J_{c(4\times3)}$ is defined by:

$$\dot{\theta} = J_{c(4\times3)}\dot{X}_c = J_e^{-1}J_o\dot{X}_c \ , \qquad (3)$$

where J_e is a block diagonal matrix composed of the Jacobian matrices of the two pantographs, $\dot{X} = J_o\dot{X}_c$, and $X = [x_1 \ y_1 \ x_2 \ y_2]^T$, the coordinates of each pantograph end-point. The mass and moment-of-inertia of the coupling linkage are represented by a diagonal matrix M with $diag(M) = [m_l \ m_l \ I_l]$, while F_h and τ are externally applied hand forces and actuator torques. The internal force acting longitudinally along the linkage bar does not affect the system dynamics since the actuator torques which constitute this force lie in the null space of J_c^T. Note that as the pantographs are oriented horizontally, there are no gravity terms. Friction is insignificant and can be neglected.

3.2 Actuation and Sensing

Four 90W DC motors provide actuation at the active pantograph joints and are considered, for the purposes of control, to be torque sources. Each of the four joint angles is measured by a digital optical encoder with a resolution of 0.09 degrees. Velocities, accelerations and forces are not directly measurable and are computed purely from joint angle measurements and applied motor torques. The relatively low resolution of these measurements presents a significant challenge to

this computation. External forces applied by the hand are derived using a system state observer [4]. Given an accurate dynamic model, as well as measured joint angles and applied actuator forces, the system states (angular joint velocity) and unknown external disturbances (hand force applied to the interface end-effector) can be observed and computed, as indicated in Figure 4. This strategy has been demonstrated for a single unarticulated body [4], but is shown here to be applicable to a parallel mechanism using a simplified Nicosia Observer [9]. Hacksel and Salcudean suggest the use of a

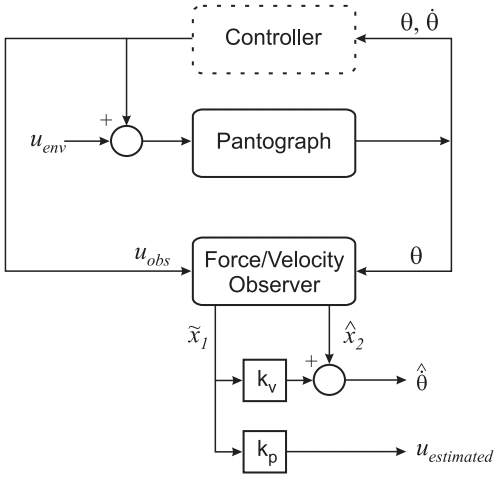

Figure 4: Force observation using only applied actuator torques and measured joint angles.

simplified Nicosia Observer for serial mechanisms [9]:

$$\begin{aligned} \dot{\hat{\theta}}_p &= \hat{\theta}_v + k_v\tilde{\theta}_p \\ \dot{\hat{\theta}}_v &= D_p(\theta)^{-1}(-C_p(\theta,\hat{\dot{\theta}}_p)\hat{\dot{\theta}}_p + k_p\tilde{\theta}_p + u_{obs}) \ , \end{aligned} \quad (4)$$

where $\hat{\theta}_p$ and $\hat{\theta}_v$ are angular position and velocity states, $\tilde{\theta}_p$ is the position state estimation error $(\theta - \hat{\theta}_p)$, k_v and k_p are state feedback gains and u_{obs} is a vector of applied actuator torques. The matrices D_p and C_p are defined in (1). In steady-state, the effective joint torques due to applied hand forces are related to angular position errors by a simple stiffness relationship, $k_p\tilde{\theta}_p$. Figure 5 shows a comparison of forces predicted off-line by an inverse dynamics model, with those estimated by the on-line force observer. The force observer clearly tracks the applied hand force closely. A relatively low observer bandwidth, limited by the coarse joint angle resolution, results in some degradation of the force and velocity observations at higher frequencies.

4 Control System Architecture

The twin pantograph interface provides the operator with a means of interacting with the virtual environment. The operator should feel the dynamics of a virtual object in free motion and environment forces during contact phases, while the operator hand force and motion should be conveyed to the virtual object. This can be achieved by adopting a two stage control strategy that consists of interface control and teleoperation control subsystems.

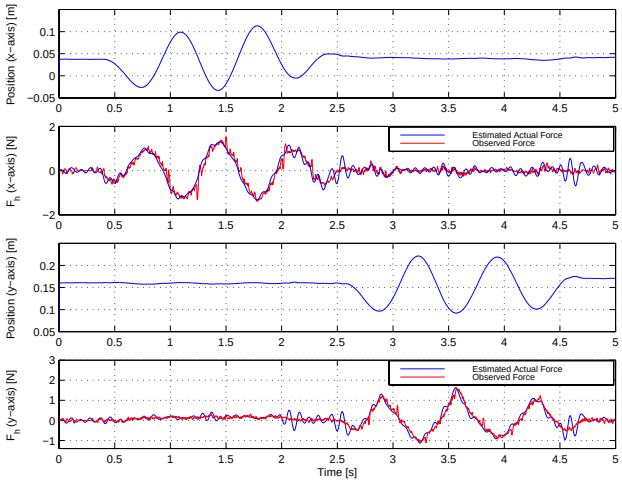

Figure 5: Force observer performance.

4.1 Interface Control

The performance achievable by the teleoperation controller is directly affected by the interface control approach. The goal is to design an impedance controller that enables one to shape the device dynamics to match any desired behaviour. This greatly simplifies teleoperation controller development.

Assuming that the desired equations of motion have the form:

$$M_d\ddot{X}_c + B_d\dot{X}_c + K_dX_c = F_h + F_m \ , \quad (5)$$

where M_d is the desired mass matrix, B_d is the desired damping matrix, K_d is the desired stiffness matrix and F_m is an external control command e.g. the sum of control commands by C_m, C_2, C_4, and C_6 in Figure 6. By combining (5) and (2), the following impedance control law is derived:

$$\begin{aligned} u =& (M_cM_d^{-1} - I)F_h + M_cM_d^{-1}F_m + \\ & (C_c - M_cM_d^{-1}B_d)\dot{X}_c - M_cM_d^{-1}K_dX_c \ . \end{aligned} \quad (6)$$

From this equation, it is clear that if the apparent mass of the device is to be changed $(M_d \neq M_c)$ then a measure of the hand force, or equivalently, the acceleration $\ddot{X}_c$ is required. The observed hand force is used to synthesise the control law. In practice this controller was able to achieve a perceived mass greater than ten times the physical mass of the device.

Once the control command u is found, it should be converted to motor torques τ. Since there is a redundancy in the actuation system, τ is not unique. Redundancy may be used to minimize the internal force applied on the connecting bar. In this case, the motor torque vector is given by

$$\tau = J_e^T J_o^{\dagger} u = J_e^T J_o (J_o^T J_o)^{-1} u \ . \qquad (7)$$

4.2 Teleoperation Control

Though our problem is primarily a haptic simulation, a tele-operation control strategy is adopted to interlink the hand controller with the virtual object. In this approach, the master is the haptic device interacting with a human operator, while the slave is replaced by the dynamic simulator software [3]. A general teleoperation architecture was proposed in [6]. It utilizes four types of data transmission between master and slave, sending forces and positions in both directions. The architecture was later modified in [5] to include the local force channels shown in Figure 6, where F_h and F_e are hand and environment forces; V_h and V_e are master and slave velocities; and Z_m, Z_s, Z_h and Z_e are master, slave, hand and environment impedances, respectively. C_1 and C_4 are position channel controllers whereas C_2, C_3, C_5 and C_6 are force channel controllers. Finally, C_m and C_s are master and slave local position-

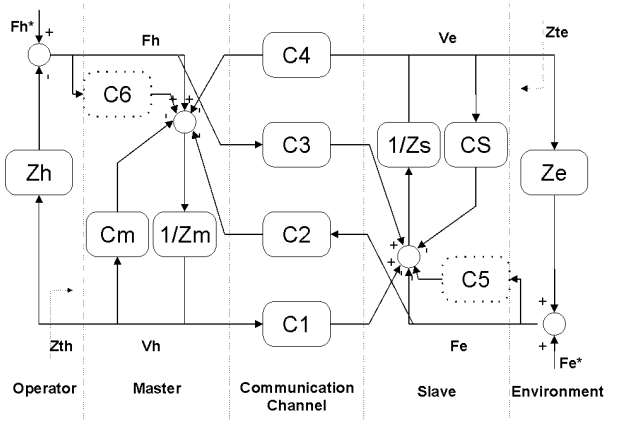

Figure 6: Four-channel architecture with local force feedback.

based controllers. In a haptic simulation, the slave and environment are virtual and the dynamic simulator replaces Z_s and Z_e. C_s is a local controller for the virtual slave, designed independently from the dynamic simulator. Z_m is the desired dynamics of the master in (5). Therefore C_m and C_6 act in addition to the impedance controller. The structure shown in Figure 6 has the following hybrid two-port network representation:

$$\begin{bmatrix} F_h \\ -V_e \end{bmatrix} = \begin{bmatrix} H_{11}(s) & H_{12}(s) \\ H_{21}(s) & H_{22}(s) \end{bmatrix} \begin{bmatrix} V_h(s) \\ F_e(s) \end{bmatrix} \qquad (8)$$

In teleoperation control design, there is always a trade-off between the achievable level of transparency and robust stability [6]. For perfect transparency,

$$H = \begin{bmatrix} Z_t & 1 \\ -1 & 0 \end{bmatrix} \ . \qquad (9)$$

In this case, the operator interacts with the environment via the tool impedance, Z_t. However, the teleoperation network optimized for transparency does not necessarily satisfy stability requirements. Llewllyn's criteria provide the necessary and sufficient conditions for system stability against any passive hand and environment impedance [1, 7]. It is not difficult to show that as long as both force gains are set to unity (i.e., $C_2 = C_3 = 1$), these requirements are not met. Once the force gains are reduced (at least one of them), the system becomes unconditionally stable unless the master and slave are identical and have no damping term. In such cases some damping must be added to the master and the slave sides.

5 Experimental Results

Different teleoperation control algorithms were implemented on the haptic device described in Section 3. Experimental results comparing their performance are presented in this section. The device was used to handle a virtual rectangular object both in free motion and in contact with a virtual wall. The impedance controller was designed to match the dynamics of the twin pantograph with the virtual object which is linear and decoupled in each coordinate. Therefore, teleoperation controllers can be designed separately for each degree of freedom. Both local impedance and the teleoperation controllers require the velocity of the master in workspace coordinates. These velocities were derived from angular velocities of the motors using the Jacobian relation (3). The angular velocities were estimated from encoder measurements using the force/velocity observer (4).

The experimental results in the y-coordinate are presented here, while similar behavior was observed in the other two coordinates. A spring model with $K = 10000$N/m was used for the virtual wall. The slave impedance was chosen as $Z_s(s) = 2s$ (a pure mass) in translation and $Z_s(s) = 0.005s$ in the angular direction. In the following experiments, local force gains C_5 and C_6 are zero.

(a) Two-channel teleoperation

In the first experiment, a two channel position-force architecture was used for haptic simulation. This is similar to an impedance simulation approach. The controller parameters were chosen as $C_1 = C_s = 40 + \frac{400}{s}$, $C_m = C_4 = 0$, $C_2 = 1$, and $C_3 = 0$. C_1 and C_s form a

position tracking controller for the virtual slave and the environment force is fed back to the master through C_2. The results are presented in Figure 7. Note that while the force tracking is good, the position tracking is lost during the contact phase which is the major drawback of this approach.

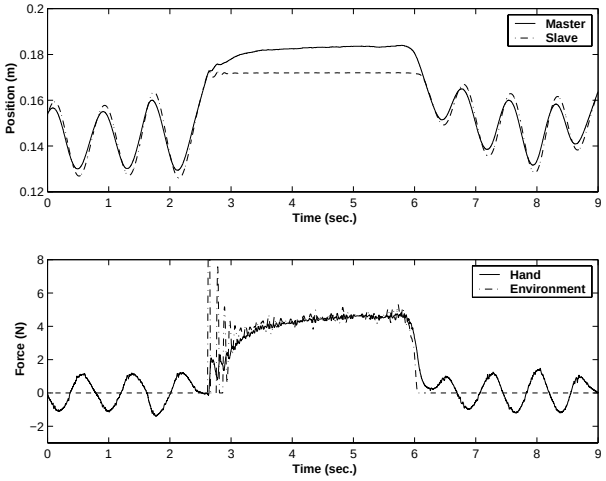

Figure 7: Two-channel position-force architecture, tracking results.

(b) Fully transparent four-channel

This experiment was conducted using $C_m = C_s = 35 + \frac{100}{s}$, $C_1 = C_s$, $C_4 = -C_m$, and $C_2 = C_3 = 1$. In fact, the enviroment and hand forces are fed forward to the master and slave with unity gains whereas a virtual spring-damper coupler is also introduced through position channels and local controllers (C_m and C_s). Figure 8 shows the position and force tracking both in free motion and during contact. Considerable chattering in contact forces is observed. However, accurate position tracking is obtained during both phases. Clearly the four-channel architecture outperforms the two channel approach in the previous experiment, at the expense of increased chattering.

(c) Four-channel with adaptive damping

To remove the force chattering observed in the previous case, an adaptive damping term was added to the slave side [10]:

$$C_s = 35 + \frac{100}{s} + B_{adp}\ ,\ B_{adp} = K_b|f_e| + B_{min}\,,$$

with $K_b = 60\text{s/m}$, $B_{min} = 0\text{kg/s}$, and f_e is the environment force. The experiment results are shown in Figure 9. The force chattering is heavily reduced whereas the position tracking is still very good.

(d) Unconditionally stable four-channel

Teleoperation controllers were chosen based upon the unconditional stability requirements where $C_m = C_s = 40 + \frac{100}{s}$, $C_1 = -C_4 = 35 + \frac{100}{s}$, and $C_2 = 0.8, C_3 = 1$.

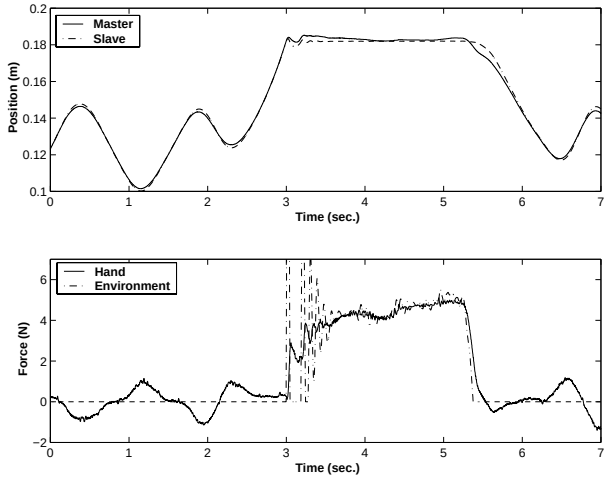

Figure 8: Fully transparent four-channel, tracking results.

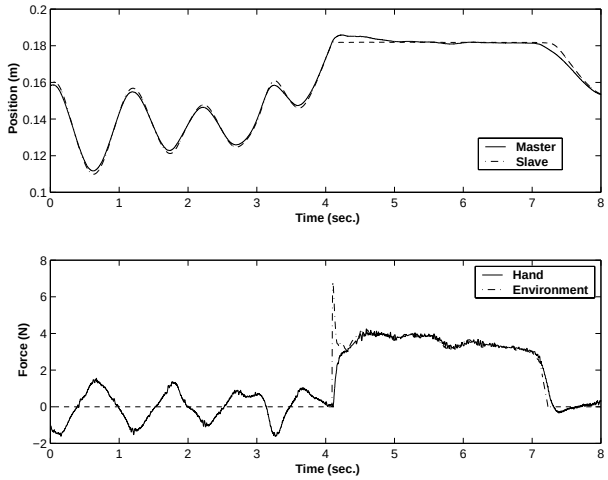

Figure 9: Four-channel with adaptive damping, tracking results.

Figure 10 shows the experimental results with this set of parameters. The force chattering is reduced at the expense of a deterioration in the system transparency, as predicted before. This is particularly evident when the object is in contact with the wall.

6 Conclusions and Future Work

This paper has outlined a novel control system design approach for haptic simulations. In an experimental virtual environment consisting of a new 3-DOF planar haptic interface, a novel force observer (based purely upon the model of the device, joint angle measurements and applied motor torques) and physically-based slave and environment models, a teleoperation control framework is shown to be effective for haptic rendering. The

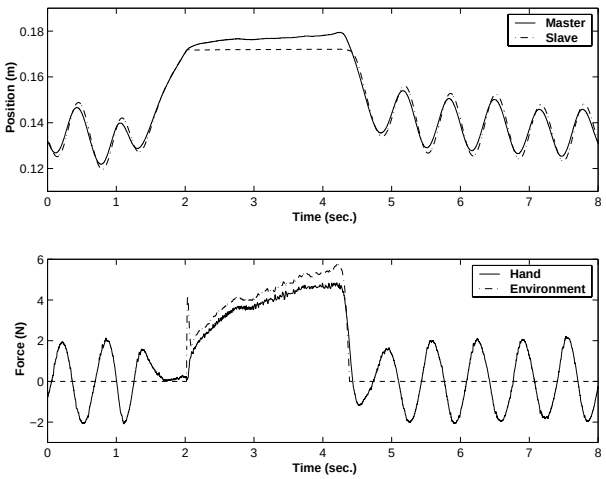

Figure 10: Unconditionally stable four-channel, tracking results.

advantage of this approach is that it provides a clear and general methodology for interactive virtual environment design. The explicit modelling of a virtual slave means that complex, multi-body and perhaps time varying slave behaviour is easily incorporated, independently of the haptic interface or its associated control system. This is in contrast to the traditional approach in which slave dynamics are implied within the haptic interface control system itself. Based on the experimental results, a four-channel teleoperation framework, augmented with adaptive damping, performs very well both in free motion and during contact phases.

Future work includes improvements and further evaluation of force observer accuracy, as well as the incorporation of more complex slave dynamics. Further optimization of the trade-off between system transparency and stability is also required of the controller design.

7 Acknowledgments

The authors would like to thank Leo Stocco and Simon Bachmann for their assistance. This work was supported by the Canadian IRIS/PRECARN Network of Centers of Excellence.

References

[1] Richard J. Adams, Manuel R. Moreyra, and Blake Hannaford. Stability and Performance of Haptic Displays: Theory and Experiments. In *Proc. of the ASME, Dynamic Systems and Control Division*, pages 227–234, Anaheim, CA, 1998.

[2] R.J. Adams and B. Hannaford. A Two-Port Framework for the Design of Unconditionally Stable Haptic Interfaces. In *Proceedings of IROS 98*, pages 1254–1259, Victoria, Canada, November 1998.

[3] D. Constantinescu, I. Chau, S. P. DiMaio, L. Filipozzi, S. E. Salcudean, and F. Ghassemi. Haptic rendering of planar rigid-body motion using a redundant parallel mechanism . In *Submitted to the International Conference on Robotics and Automation*, 2000.

[4] P.J. Hacksel and S.E. Salcudean. Estimation of Environment Forces and Rigid-Body Velocities using Observers. In *Proceedings of the IEEE International Conference on Robotics and Automation*, pages 931–936, San Diego, CA, May 1994.

[5] K. Hashtrudi-Zaad and S.E. Salcudean. On the Use of Local Force Feedback for Transparent Teleoperation. In *IEEE International Conference on Robotics and Automation*, pages 1863–1869, Detroit, MI, May 1999.

[6] D.A. Lawrence. Stability and Transparency in Bilateral Teleoperation. In *IEEE Transactions on Robotics and Automation*, volume 9, pages 624–637, 1993.

[7] F.B. Llewellyn. Some Fundemental Properties of Transmission Systems. In *Proc. IRE*, pages 271–283, 1952.

[8] A. Nahvi, D.D. Nelson, J.M. Hollerbach, and D.E. Johnson. Haptic Manipulation of Virtual Mechanisms from Mechanical CAD Designs. In *Proceedings of the 1998 IEEE International Conference on Robotics and Automation*, pages 375–380, Leuven, Belgium, May 1998.

[9] S. Nicosia and P. Tomei. Robot control by using only joint position measurements. In *IEEE Transactions on Automatic Control*, pages 1058–1061, September 1990.

[10] S.E. Salcudean, M. Wong, and R.L. Hollis. Design and Control of a Force-Reflecting Teleoperation System with Manetically Leviated Master and Wrist. In *IEEE Trans. on Robotics and Automation*, volume 11, December 1995.

[11] Septimiu E. Salcudean. Control for Teleoperation and Haptic Interfaces. In B. Siciliano and K. P. Valavanis, editors, *Lecture Notes in Control and Information Sciences 230 – Control Problems in Robotics and Automation*, pages 51–65. Springer-Verlag, 1997.

[12] Mark W. Spong and M. Vidyasagar. *Robot Dynamics and Control*. Wiley, 1989.

[13] T. Yoshikawa and H. Uead. Construction of Virtual World Using Dynamics Modules and Interaction Modules. In *Proceedings of the 1996 IEEE International Conference on Robotics and Automation*, pages 2358–2364, Minneapolis, Minnesota, 1996.